Monthly Runoff Forecasting Using Variational Mode Decomposition Coupled with Grey Wolf Optimizer Based Long Short-term Memory Neural Networks

Bao-Jian Li (libaojian@ncwu.edu.cn)
North China University of Water Resources and Electric Power
Guo-Liang Sun
North China University of Water Resources and Electric Power
Yan Liu
Zhengzhou University of Light Industry
Wen-Chuan Wang
North China University of Water Resources and Electric Power
Xu-Dong Huang
North China University of Water Resources and Electric Power

Research Article

Keywords: variational mode decomposition, long short-term memory neural networks, gray wolf optimizer, monthly runoff forecasting

Posted Date: January 17th, 2022

DOI: https://doi.org/10.21203/rs.3.rs-1018857/v1

Monthly Runoff Forecasting Using Variational Mode Decomposition Coupled with Grey Wolf Optimizer Based Long Short-term Memory Neural Networks

Bao-Jian, Li[1,2,*], Guo-Liang, Sun[1], Yan, Liu[3], Wen-Chuan, Wang[1,2], Xu-Dong, Huang[1,2]

1 School of Water Resources, North China University of Water Resources and Electric Power, Zhengzhou 450046, China;

2 Henan Key Laboratory of Water Resources Conservation and Intensive Utilization in the Yellow River Basin, Zhengzhou 450046, China

3 College of Computer and Communication Engineering, Zhengzhou University of Light Industry, Zhengzhou 450066, China;

Abstract: Accurate and reliable monthly runoff forecasting plays an important role in making full use of water resources. In recent years, long short-term memory neural networks (LSTM), as a deep learning technology, has been successfully applied in forecasting monthly runoff. However, the hyperparameters of LSTM is predetermined, which has a significant influence on model performance. In this study, given decomposition of monthly runoff series may provide more accurate predication revealed by many previous studies, a hybrid model, namely VMD-GWO-LSTM, has been proposed for monthly runoff forecasting. The proposed hybrid model is comprised of two main components, namely variational mode decomposition (VMD) coupled with grey wolf optimizer (GWO) based LSTM. First, VMD is utilized to decompose raw monthly runoff series into several subsequences. Second, GWO is implemented to optimize the hyperparameters of LSTM for each subsequence on condition that the inputs are determined. Finally, the total output of all subsequences is aggregated as final forecast result. Four quantitative indexes are employed to evaluate the model performance. The proposed model is demonstrated using monthly runoff series data derived from two reservoirs in China's Pearl River system. To identify the feasibility and superiority of the proposed model, back propagation neural networks (BPNN), support vector machine (SVM), LSTM, EMD-LSTM, VMD-LSTM and GWO-LSTM are also utilized for comparison. The results indicate that the proposed hybrid model can yield best forecast accuracy among these models, making it a promising new method for monthly runoff forecasting.

Keywords: variational mode decomposition, long short-term memory neural networks, gray wolf optimizer, monthly runoff forecasting

*corresponding author
E-mail address: libaojian@ncwu.edu.cn (B.-J. Li).

1. Introduction

Accurate and reliable monthly runoff forecasting plays an important role in water resources management, such as water supply (Şen, 2021), hydroelectric generation (Feng et al., 2020a) and ecological restoration (Feng et al., 2018). Generally, existing methods can be approximately partitioned into data-driven (Feng et al., 2021; Liao et al., 2020; Wang et al., 2015), and physical-based models (Dakhlalla and Parajuli, 2016; Liao et al., 2016; Madsen, 2003). The data-based models can simulate the relationship between input and output without regard to complex mechanisms of runoff generation (Niu et al., 2019). As a contrast, the physical-based models take into account specific physical process and demand mass data such as underlying surface conditions, human activity influence and climate change which are not easily collected (Feng and Niu, 2021). Unlike the physical-based models, the data-based models demand less data and can afford satisfactory forecast results. As a typical representative of data-based models, artificial neural networks (ANN) has been widely and successfully utilized in hydrology-related areas, for instance, precipitation forecasting (Nourani et al., 2009), runoff forecasting (Shoaib et al., 2018), water level forecasting (Seo et al., 2015), etc. In the past few decades, numerous ANN architectures and algorithms have been investigated in hydrological time series forecasting (ASCE-Task-Committee, 2000).

Long short-term memory neural networks (LSTM) proposed by Hochreiter and Schmidhuber (Hochreiter and Schmidhuber, 1997) is a special kind of recurrent neural network (RNN) and has merits of fast convergence and good nonlinear predictive capability. To avoid the problems of training long sequences and vanishing gradients faced by the traditional RNN, LSTM implements constant error flow via constant error carrousels within special memory cells. Referred to LSTM, many literatures have been studied in hydrological time series forecasting (Lv et al., 2020; Ni et al., 2020; Wang et al., 2021). Nevertheless, the hyperparameters of LSTM are predetermined, which has a certain impact on forecast accuracy. In general, there are two main methods to improve the forecast accuracy in the previous studies. The first is to combine decomposition algorithms to decompose original time series data into several subcomponents, employ LSTM to simulate each subcomponent, and aggregate the result of each subcomponent as the final result (Lv et al., 2020). Zuo et al. (Zuo et al., 2020), for example, proposed a single-model forecasting based on VMD and LSTM to predict daily streamflow 1-7 days ahead, and investigated the robustness and efficiency of the proposed model for forecasting highly nonstationary and nonlinear streamflow. The Second is to utilize optimization algorithms to optimize the

hyperparameters of the LSTM (ElSaid et al., 2018). Yuan et al. (Yuan et al., 2018), for example, used ant lion optimizer (ALO) to calibrate the parameters of the LSTM, and verified its effectiveness with the historical monthly runoff of the Astor River Basin. At present, there are several commonly used decomposition algorithms (Colominas et al., 2014; Roushangar et al., 2021; Shahid et al., 2020), for instance, wavelet decomposition, empirical mode decomposition (EMD) and VMD. The optimization algorithms, such as particle swarm optimization and ant colony optimization, can be seen in the literature as optimizing the parameters of neural networks (Wan et al., 2017; Yu et al., 2008). In this study, both methods are considered.

Variational mode decomposition (VMD) (Dragomiretskiy and Zosso, 2014) is an entirely non-recursive variational model that can extract modes concurrently. Via VMD, a signal can be decomposed into a sequence of subcomponents with different frequency bands and time resolutions (Fang et al., 2019). Compared to empirical mode decomposition (EMD), VMD is capable of separating tones of similar frequencies. VMD has been widely applied in many research fields, such as fault diagnosis (Zhang et al., 2017), signal processing (Wang et al., 2017), wind speed monitoring (Liu et al., 2018) and hydrological time series forecasting (Feng et al., 2020b; Li et al., 2021; Sibtain et al., 2021). In this study, VMD was selected as a data preprocessing tool to decompose monthly run off series. In recent years, an emerging swarm intelligence algorithm called grey wolf optimizer (GWO) has been proposed, which imitates the social hierarchy and hunting behavior of grey wolves (Mirjalili et al., 2014). With its strong robustness and searching ability in solving optimization problem, GWO has been widely and successfully applied in many fields, like model parameter calibration (Tikhamarine et al., 2020), reservoir operation (Niu et al., 2021) and optimal power dispatch (Nuaekaew et al., 2017). In view of its strong robustness and searching ability, GWO can be adopted to optimize the hyperparameters of LSTM. In this paper, a hybrid model, referred to as VMD-GWO-LSTM, is proposed for monthly runoff forecasting. According to the monthly runoff series of two real-world hydropower reservoirs in China, the proposed method is certified to be feasible. The novel contributions of this study can be stated as follows. (1) To decrease modeling difficulty, VMD is adopted to decompose monthly runoff series into several simple subcomponents. (2) For each subcomponent, the input-output relationships are identified by LSTM and the GWO method is employed to optimize the hyperparameters of LSTM. (3) The results of case study indicate that, compared to several traditional models, the proposed hybrid method VMD-GWO-LSTM can yield better

forecast accuracy. To our knowledge, there are few studies about combining VMD, LSTM, and GWO to forecast monthly runoff, demonstrating this study has the potential to refill this gap.

The rest of this work is organized as follow: Section 2 describes the details of the proposed approach; in Section 3, the proposed method is utilized to forecast the monthly runoff of two reservoirs; finally, the conclusions are summarized.

2 Methodology

2.1 Variational mode decomposition

VMD is a novel variational method which can non-recursively decompose a nonstationary signal into a given number of mode functions and each individual mode is compact around its center frequency (Dragomiretskiy and Zosso, 2014). To obtain each mode and its center frequency, a constrained variational problem can be expressed as follows:

$$\begin{cases} \min\limits_{\{u_k(t)\},\{\omega_k(t)\}} \left\{ \sum\limits_k \left\| \partial_t \left[\left(\delta(t) + \dfrac{j}{\pi t} \right) * u_k(t) \right] e^{-j\omega_k t} \right\|_2^2 \right\} \\ s.t. \sum\limits_k u_k(t) = f(t) \end{cases} \tag{1}$$

where t is the time step; $u_k(t)$ and $\omega_k(t)$ denote k-th mode and its corresponding center frequency, respectively; $\delta(t)$ is the Dirac distribution, * denotes the convolution calculation and $f(t)$ denotes the t-th data of the input signal.

In order to facilitate solution, the quadratic penalty factor α and the Lagrangian multiplier λ are introduced to transform the constrained variational problem into an unconstrained variational problem. Hence, the augmented Lagrangian structure can be expressed as follows:

$$L\left(\{u_k\},\{\omega_k\},\lambda\right) = \alpha \sum_k \left\| \partial_t \left[\left(\delta(t) + \frac{j}{\pi t} \right) * u_k(t) \right] e^{-j\omega_k t} \right\|_2^2 + \left\| f(t) - \sum_k u_k(t) \right\|_2^2 + \left\langle \lambda(t), f(t) - \sum_k u_k(t) \right\rangle \tag{2}$$

where $\langle \cdot \rangle$ represents the inner product operation.

The Eq. (2) can then be solved by the alternating direction method of multiplier (ADMM) to get the saddle point of the augmented Lagrangian function. In the ADMM, the variables ($\hat{u}_k^{n+1}$, ω_k^{n+1} and $\hat{\lambda}^{n+1}$) are continuously updated to optimize each modal component. And thus the optimal individual mode u_k and the corresponding center frequency ω_k can be obtained by the iterative equation expressed as follows:

$$\hat{u}_k^{n+1}(\omega) = \frac{\hat{f}(\omega) - \sum\limits_{i \neq k} \hat{u}_i(\omega) + \dfrac{\hat{\lambda}(\omega)}{2}}{1 + 2\alpha(\omega - \omega_k)^2} \tag{3}$$

$$\omega_k^{n+1} = \frac{\int_0^\infty \omega \left|\hat{u}_k(\omega)\right|^2 d\omega}{\int_0^\infty \left|\hat{u}_k(\omega)\right|^2 d\omega} \tag{4}$$

$$\hat{\lambda}^{n+1}(\omega) = \hat{\lambda}^n(\omega) + \tau\left(\hat{f}(\omega) - \sum_k \hat{u}_k^{n+1}(\omega)\right) \tag{5}$$

where n is the iteration number; τ is the iterative factor; $\hat{f}(w)$, $\hat{u}_i(w)$, $\hat{\lambda}(w)$ and $\hat{u}_k^{n+1}$ denote the Fourier transforms of $f(t)$, $u_i(t)$, $\lambda(t)$ and $\hat{u}_k^{n+1}(t)$, respectively.

2.2 long short-term memory neural networks

As a type of deep learning neural networks, LSTM was proposed to overcome the gradient vanishing/exploding problem faced by traditional RNN (Hochreiter and Schmidhuber, 1997). LSTM takes place of the conventional hidden unit with a memory cell and contains multiple memory blocks of which each include three gates: input gate, forget gate and output gate and at least a memory cell. By LSTM, information from the three gates can be added or deleted to the memory cell state. Based on the previous state, current memory and current input, the LSTM owns the ability to decide which cells are restrained and promoted and on the basis of the three gates what information is saved and forgotten during the training process (Altan et al., 2021). The structure of LSTM is shown in Fig. 1. For the three gates: the multiplicative input gate unit is employed to recognize new information that can be gathered in the cell; the multiplicative output gate unit is utilized to compute the information that can be propagated to the network; the multiplicative forget gate unit is used to decide whether the last status of the cell can be forgotten (Li et al., 2018).

Insert Here Fig. 1

The calculation of the three gates and cell state can be generally expressed as follows:

$$\begin{aligned}
f_t &= \sigma\left(W_f \cdot \left[h_{t-1}, x_t\right] + b_f\right) \\
i_t &= \sigma\left(W_i \cdot \left[h_{t-1}, x_t\right] + b_i\right) \\
\&\%_t &= \tanh\left(W_c \cdot \left[h_{t-1}, x_t\right] + b_c\right) \\
c_t &= f_t \text{ e } c_{t-1} + i_t \text{ e } \&\%_t \\
o_t &= \sigma\left(W_o \text{ e } \left[h_{t-1}, x_t\right] + b_0\right) \\
h_t &= o_t \cdot \tanh\left(c_t\right)
\end{aligned} \tag{5}$$

where f_t, i_t, o_t denote the output of the forget gate, input gate and output gate, respectively; $\&\%_t$ is the potential cell state; c_t and h_t denote the cell state and cell output at the time *t*; W_f, W_i, W_c W_o and b_f, b_i, b_c, b_0 denote weight matrices and the corresponding bias vectors; x_t is the input at time *t*, σ is the sigmoid function; e denotes matrix multiplication.

It is worth noting that LSTM relies heavily on a set of hyperparameters to achieve good performance, which usually requires a certain amount of practical experience to manually select and optimize the hyperparameters. Therefore, for convenience, automatic algorithmic approaches with ability to converge faster and gain an optimal/ near optimal solution within an acceptable time can be employed to enhance the performance of LSTM (Nakisa et al., 2018).

2.3 Grey wolf optimizer

The GWO algorithm is a novel swarm intelligent optimization algorithm that simulates the leadership hierarchy and predation strategy of grey wolves (Mirjalili et al., 2014). Grey wolves possess the very strict social dominant hierarchy, which can be divided into four categories including alpha wolf (α), beta wolf (β), delta wolf (δ) and omega wolf (ω). The alpha dominates the whole wolf pack and is responsible for making decisions. Beta wolves are subordinate to the alpha in the hierarchy, but command delta and omega wolves as well. Meanwhile, alpha wolves are also responsible for coordinating alpha wolves to make decisions. Delta wolves obey the orders of alpha and beta wolves and are responsible for the detection and guarding of the wolf pack. The omega is the lowest ranking and omega wolves play a vital role in the balance of internal relationships among the pack. The hunting process of grey wolves can be divided into three stages: (i) tracking, chasing and approaching prey; (ii) hunting, surrounding and intruding the prey until it stops moving; (iii) attacking the prey (Mirjalili et al., 2014). The optimal solution is obtained by updating and evolving the positions of wolves, and gradually approaching the prey. The GWO algorithm can be roughly described as follows.

Firstly, encircling prey is carried out by the grey wolves before hunting process, which can be defined as follows:

$$\vec{D} = \left| \vec{C} \cdot \vec{X}_p(t) - \vec{X}(t) \right| \tag{6}$$

$$\vec{X}(t+1) = \vec{X}(t) - \vec{A} \cdot \vec{D} \tag{7}$$

$$\vec{A} = 2\vec{a} \cdot \vec{r}_1 - \vec{a} \tag{8}$$

$$\vec{C} = 2 \cdot \vec{r}_2 \tag{9}$$

where t is the current iteration; $\vec{D}$ is the distance between the grey wolf and the prey; $\vec{X}_P(t)$ is the position vector of the t-th prey; $\vec{X}(t)$ is the position vector of the t-th grey wolf; $\vec{A}$ and $\vec{C}$ are coefficient vectors; $\vec{r}_1$ and $\vec{r}_2$ are random numbers in [0,1]; $\vec{a}$ is transition parameter and linearly reduced from 2 to 0 during the iterative computation.

Then, hunting process is implemented. After recognizing the position of the prey and encircling them, the wolves will hunt the prey which is guided by the alpha and the beta and delta participating occasionally. In this process, it is assumed that the alpha has best candidate solution and the top three solutions have better knowledge about the potential position of prey. Hence, the formulas are given as follows which other wolves should be obeyed to update their positions:

$$\begin{cases} \vec{D}_\alpha = \left| \vec{C}_1 \cdot \vec{X}_\alpha - \vec{X} \right| \\ \vec{D}_\beta = \left| \vec{C}_2 \cdot \vec{X}_\beta - \vec{X} \right| \\ \vec{D}_\delta = \left| \vec{C}_3 \cdot \vec{X}_\delta - \vec{X} \right| \end{cases} \tag{10}$$

$$\begin{cases} \vec{X}_1 = \vec{X}_\alpha - A_1 \cdot \vec{D}_\alpha \\ \vec{X}_2 = \vec{X}_\beta - A_2 \cdot \vec{D}_\beta \\ \vec{X}_3 = \vec{X}_\delta - A_3 \cdot \vec{D}_\delta \end{cases} \tag{11}$$

$$\vec{X}(t+1) = \frac{\vec{X}_1 + \vec{X}_2 + \vec{X}_3}{3} \tag{12}$$

Finally, attacking prey is executed. In order to simulate being close to the prey, the value of $\vec{a}$ is decreased linearly and correspondingly the fluctuation range of $\vec{A}$ is also decreased within the interval of [-2a, 2a]. When $\vec{A}$ ranging in [-1, 1], the next position of a grey wolf in any position is between its current position and the position of the prey (Mirjalili et al., 2014). And thus the attack on the prey can be realized.

2.4 Hybrid model for monthly runoff forecasting

Hydrological time series with the characteristics of nonlinearity and nonstationarity are usually related to various factors, including climate change and variation of underlying surface conditions (Ji et al., 2014; Xu et al., 2017). To improve forecast accuracy of monthly runoff forecasting, a hybrid model shortened to VMD-GWO-LSTM is proposed and illustrated in Fig.2. Firstly, VMD is utilized to decompose the original complex runoff time series into several relatively simple subsequences. Secondly, LSTM of which the hyperparameters are optimized by GWO, is employed to simulated each subsequence. Finally, the simulation results of all subsequences are aggregated as the final forecast result. The main procedure can be described as follows:

Step 1: Data preprocessing. Utilize VMD to decompose the original runoff sequence to obtain K subsequences with different frequencies. All subsequences that are divided into calibration and validation data are normalized to [-1,1].

Step 2: Input determination. Utilize partial autocorrelation function (PACF) to determine the inputs

variables of each subsequence for the LSTM model.

Step 3: Hyperparameter optimization. The GWO algorithm of which root-mean-squared error (RMSE) is selected as an optimization criterion, is carried out independently to optimize the hyperparameters of the LSTM model for simulating each subsequence. In this study, the optimal parameters of the number of hidden layer neurons, the number of epochs and the learning rate of the LSTM model are searched.

Step 4: Aggregation. The forecast results of all subsequences are arithmetically aggrated as the final forecast results.

Insert Here Fig. 2

2.5 Evolution index

Selecting appropriate evaluation criteria is essential for utilizing multi-criteria analysis to validate model performance (Modarres, 2009). In this section, four evolution indexes, namely RMSE, mean absolute percentage error (MAPE), coefficient of correlation (R) and Nash-Sutcliffe efficiency coefficient (CE) are employed. Generally, the smaller RMSE and MAPE and the higher R and CE, the better model performance. These indexes as listed as below:

$$RMSE = \sqrt{\frac{1}{n}\sum_{i=1}^{n}(Q_i - \hat{Q}_i)^2} \tag{13}$$

$$MAPE = \frac{1}{n}\sum_{i=1}^{n}\left|\frac{Q_i - \hat{Q}_i}{Q_i}\right| \times 100 \tag{14}$$

$$R = \frac{\sum_{i=1}^{n}(Q_i - \bar{Q}_i)(\hat{Q}_i - \bar{\hat{Q}}_i)}{\sqrt{\sum_{i=1}^{n}(Q_i - \bar{Q}_i)^2 \sum_{i=1}^{n}(\hat{Q}_i - \bar{\hat{Q}})^2}} \tag{15}$$

$$CE = 1 - \frac{\sum_{i=1}^{n}(Q_i - \bar{Q}_i)^2}{\sum_{i=1}^{n}(Q_i - \bar{Q})^2} \tag{16}$$

where n is the number of observed data; Q_i and $\hat{Q}_i$ are the observed and forecasted values, respectively; $\bar{Q}_i$ and $\bar{\hat{Q}}_i$ are the averages of all observed and forecasted values, respectively.

3 Case studies

3.1 Study area and data

Two multipurpose Reservoirs, the Xinfengjiang and Guangzhao Reservoirs illustrated in Fig. 3, were

selected as case studies. The Xinfengjiang Reservoir is located on the Xinfeng River, which is the largest tributary of the Dongjiang River, a second-level tributary of the Pearl River. With 336.1 MW of installed capacity and 13.896 billion m^3 of storage volume as well as 5740km^2 of drainage area, the Xinfengjiang Reservoir is the largest Reservoir in the south of China. For the Xinfengjiang Reservoir, the primary goal is power generation. The Guangzhao Reservoir is located on the middle reaches of the Beipan River, which is a tributary of the Xijiang River, a second-level tributary of the Pearl River. With 1040MW of installed capacity and 3.245 billion m^3 of storage volume as well as 13548km^2 of drainage area, the primary goal of the Guangzhao Reservoir is power generation. Hence, accurate monthly runoff forecasting is vital for these two reservoirs.

Monthly runoff series data from the Xinfengjiang and Guangzhao Reservoirs were retrieved for validating the proposed method. The monthly runoff hydrograph of the two reservoirs is depicted in Fig. 4, where the data for Xinfengjiang covers from 1943 to 2015 and the data for Guangzhao covers from 1956 to 2017. It can be seen that the monthly runoff for the two reservoirs varies over a wide range. For these two reservoirs, approximate 70% of the data was used for calibration and the remaining was used for validation.

Insert Here Fig. 3

Insert Here Fig. 4

3.2 Decomposition results

According to VMD, the key parameter of the number of mode should be predefined, which affects the decomposed results (Wen et al., 2019). To obtain satisfactory performance, the traditional EMD method was employed to ascertain the number of subsequences. The decomposed results for the Xinfengjiang and Guangzhao Reservoirs utilizing VMD and EMD are shown in Figs. 5 and 6, respectively. It can be found that there are significant differences in the acquired subcomponents for the two reservoirs, which indicate the variability of VMD and EMD in the aspect of extracting intrinsic information from original monthly runoff series.

Insert Here Fig. 5

Insert Here Fig. 6

3.3 Input determination

The selection of input variables that directly affects the forecast results, should be predetermined. As a statistical method, partial the partial autocorrelation function (PACF) can be employed to analysis and

246 determine the input variables (Feng et al., 2020; He et al., 2019). In practice, the input variables are often
247 determined by means of the PACF values that the pervious values are selected as inputs when all PACF
248 values fall into the confidence interval. The PACF values for the original and decomposed subsequences
249 of Xinfengjiang Reservoir data are shown in Figs. 7 and 8. On the basis of Figs. 7 and 8, the input
250 variables for each sequences of Xinfengjiang and Guangzhao Reservoirs data can be determined. From
251 Tables 1 and 2, it can be easily seen that the number of the input variables for the original and decomposed
252 data are similar, but not always the same, indicating the complex and variable features of the data from
253 the two reservoirs.

254 Insert Here Fig. 7

255 Insert Here Fig. 8

256 Insert Here Table 1

257 Insert Here Table 2

258 **3.4 Model development**

259 To confirm the feasibility of the proposed method, five models were employed for comparison, namely
260 back propagation neural networks (BPNN), support vector machine (SVM), LSTM, VMD-LSTM and
261 EMD-LSTM models. The details of the models are stated as follows.

262 (1) BPNN model

263 The original monthly runoff data were used to calibrate the parameters of BPNN model. In this study,
264 for the two reservoirs, three layers feedforward neural networks were employed, of which the input nodes
265 were set based on PACF values of the original series and each sub-series, the output nodes were set as 1
266 and the hidden nodes were set by trial-and-error procedure.

267 (2) SVM model

268 The original monthly runoff data were used to calibrate the parameters of SVM model. In this study,
269 the radial basis function was chosen as the kernel function, and the genetic algorithm was used to
270 optimize the parameters of SVM model.

271 (3) LSTM model

272 Similar to the LMNN and SVM models, the original monthly runoff data were used to calibrate the
273 parameters of LSTM model. The number of hidden layers is 2. For the LSTM model, the input nodes
274 were set based on PACF values of the original series and each sub-series, the output nodes were set as 1
275 and the hidden units for each hidden layer were set by trial-and-error procedure. In addition, the

hyperparameters, i.e. epoch and learning rate, were also set by trial-and-error procedure.

(4) VMD-LSTM and EMD-LSTM models

For the VMD-LSTM and EMD-LSTM models, there are there three main steps to be implemented. Firstly, the original monthly runoff data were decomposed into several subsequences using VMD or EMD. Secondly, the standard LSTM model was employed to simulate each subsequence and the input variables for each subsequence are listed in Tables 1 and 2. Finally, the results for each subsequence were aggregated as the final results.

3.5 Forecast results

3.5.1 Results for the Xinfengjiang Reservoir

According to the methods aforementioned, the original monthly runoff series and extracted subsequences were simulated. The detailed evaluation indexes of different models over the calibration and validation periods for the Xinfengjiang Reservoir is presented in Table 3. It can be intuitively found that compared with BPNN, SVM, LSTM, EMD-LSTM and VMD-LSTM models, the VMD-GWO-LSTM can yield the best results in terms of all the four evolution indexes both in calibration and validation periods. For instance, compared with the standalone BPNN model, the proposed hybrid VMD-GWO-LSTM model can respectively provide better forecast accuracy with decrement of 77.95% and 75.57% in terms of RMSE and MAPE and increment of 81.67% and 397.93% in terms of R and CE during the validation period. As can be seen in Table 3, the hybrid models, such as EMD-LSTM and VMD-LSTM, comprised of LSTM and decomposed methods outperform the standalone LSTM model in terms of all the four evolution indexes during the calibration and validation periods. For example, compared with the LSTM method, the VMD-LSTM model performs better with decrement of 72.06% and 57.51% in terms of RMSE and MAPE and increment of 52.66% and 154.96% in terms of R and CE during the validation period. In addition, Table 3 also reveals that the proposed hybrid model VMD-GWO-LSTM performs slightly better than the VMD-LSTM model in terms of the four measures both in the calibration and validation periods.

Insert Here Table 3

To detect the performance of tracing dynamic changes of the monthly runoff, a comparison of forecasted versus observed runoff data using BPNN, SVM, LSTM, EMD-LSTM, VMD-LSTM and VMD-GWO-LSTM for the Xinfengjiang Reservoir is depicted in Fig.9. On the whole, all of the models can simulate monthly runoff to some extent except for significant difference existed in peak flow

prediction, indicating different models with different abilities in simulating peak runoff. To comprehend the performance of the models, the scatter diagrams for the Xinfengjiang Reservoir are presented in Fig.10, which shows less scatters with VMD-GWO-LSTM than the other five models and are consistent with the results in Table 3.

Insert Here Fig. 9

Insert Here Fig. 10

Insert Here Table 4

In addition, to assess the performance of the proposed hybrid mode in peak flow forecasting, peak flow estimates of different models over the validation period for the Xinfengjiang Reservoir can be proceeded by statistical analysis. As shown in Table 4, the absolute average of the relative error of the BPNN, SVM, LSTM, EMD-LSTM, VMD-LSTM and VMD-GWO-LSTM for forecasting the 21 peak flows are 38.9%, 46.0%, 43.7%, 23.2%, 10.8% and 9.4%, respectively. It can be easily concluded that in the aspect of peak flow forecast, the VMD-GWO-LSTM model can yield much better forecast accuracy than BPNN, SVM, LSTM and EMD-LSTM, and outperform slightly better forecast than the VMD-LSTM.

3.5.2 Results for the Guangzhao Reservoir

The statistics of different models over the calibration and validation periods for the Guangzhao Reservoir is shown in Table 5. It can be easily seen that the hybrid methods, namely, EMD-LSTM, VMD-LSTM and VMD-GWO-LSTM display better performance than the standalone BPNN, SVM and LSTM. Furthermore, Table 5 also reveals that forecast accuracy of the LSTM model can be enhanced under the condition of optimized hyperparameters. For instance, compared to the SVM model, the VMD-LSTM can respectively provide better forecast accuracy with decrement of 59.06% and 65.66% in terms of RMSE and MAPE and increment of 31.73% and 80.51% in terms of R and CE during the validation period; compared to the VMD-LSTM model, the VMD-GWO-LSTM model can respectively provide better forecast accuracy with decrement of 36.13% and 21.39% in terms of RMSE and MAPE and increment of 2.61% and 5.34% in terms of R and CE during the validation period. Hence, it reconfirms that the proposed hybrid model is superior to the other models utilized in this study.

Insert Here Table 5

The forecast results of different models for the Guangzhao Reservoir during the validation phrase are drawn in Fig.11. It is clear from the hydrographs that the BPNN model having the worst performance of tracing dynamic changes of the monthly runoff and the rest models can afford satisfactory forecast results.

The scatter diagrams for the Guangzhao Reservoir are plotted in Fig.10. It can be intuitively found that the VMD-GWO-LSTM model can offer the least forecast results among the six models and display the best performance with a trendline very near to the observed data line.

Insert Here Fig. 11

Insert Here Fig. 12

Table 6 lists the statistics of peak flow estimates of different models for the Guangzhao Reservoir during the validation period. From Table 6, the absolute average of the relative error of the BPNN, SVM, LSTM, EMD-LSTM, VMD-LSTM and VMD-GWO-LSTM models for forecasting the 18 peak flows are 31.4%, 33.2%, 31.7%, 15.8%, 7.6% and 6.2%, respectively. Thus, in terms of peak flow forecast, the VMD-GWO-LSTM model can perform much better than the BPNN, SVM, LSTM and EMD-LSTM models, and slightly better than the VMD-LSTM model. As a consequence, the VMD-GWO-LSTM model is an efficient method for monthly runoff forecasting ascribing its superior performance over the comparable models during the validation period.

Insert Here Table 6

3.6 Discussion

According to the forecast results provided by BPNN, SVM and LSTM, it can be directly found that there are significant differences in terms of the four evolution indexes, demonstrating the importance of model selection and model parameter calibration. For the BPNN model, the gradient-based training algorithms have to face some drawbacks, such as over-fitting and local optimum (Wu and Chau, 2011). The ordinary SVM employing the structural risk-minimization principle can obtain good generalization performance. Nonetheless, the performance of SVM usually relies on the optimization algorithm to optimize the parameters and many studies can be referred in the literature (Feng et al., 2020b). As a deep learning algorithm, LSTM can overcome the gradient vanishing/exploding problem faced by traditional RNN and exhibit good generalization performance in hydrological time series prediction (Kratzert et al., 2018). Influenced by many factors such as human activities and climate changes, runoff usually contains multifrequency components (Niu et al., 2019). Hence, it is difficult to use a standalone prediction model to completely simulate runoff precisely because only one resolution component is used and the underlying multi-scale phenomena can’t be unraveled. As decomposition methods, EMD and VMD are utilized to identify the multifrequency components to decrease the modelling difficulty. Therefore, the EMD-LSTM and VMD-LSTM models performed better than the standalone LSTM. Although many

successful applications of LSTM have not involved how to optimize the hyperparameters, it is still worth paying much attrition to the hyperparameter optimization to enhance model performance and swarm intelligent algorithms (i.e., GWO) can be selected as possible solutions. Consequently, the proposed model VMD-GWO-LSTM outperformed the VMD-LSTM model.

The probable causes of VMD-GWO-LSTM superior to the comparable models can be generally attributed to the contribution of VMD decomposition and hyperparameters optimization based on GWO for LSTM. VMD can decompose the monthly runoff time series into several subsequences and ravel the underlying multi-scale phenomena implied in the monthly runoff time series. Each subsequence was simulated by LSTM with hyperparameters optimization conducted by GWO, which can identify the dynamic changes and decrease the modelling difficulty. Meanwhile, automatic optimization of hyperparameters of LSTM conquers the drawbacks of presetting parameters easily causing to lower forecast accuracy.

Although the feasibility of VMD-GWO-LSTM has been verified with monthly runoff data derived from two reservoirs, further research should be made in the future. It is necessary to involve new and excellent decomposition algorithms to enhance the quality of subsequences. Of course, more machine learning techniques should be investigated and verified to improve the single model forecast accuracy. Furthermore, the standard swarm optimization algorithms, for example GWO used in this study, should be modified to improve the quality of parametric optimization for the models.

4 Conclusion

In this study, a hybrid model, VMD-GWO-LSTM for short, has been proposed for forecasting monthly runoff. Firstly, the original monthly runoff data is decomposed into several subsequences. Secondly, each subsequence is simulated by a standalone LSTM model, of which the hyperparameters, including learning rate, epochs and hidden layer neurons, are optimized by GWO. Finally, all of the output of the standalone LSTM for each subsequence are aggregated as the final forecast results. Monthly runoff data derived from two reservoirs (Xinfengjiang and Guangzhao Reservoirs) located in China were employed to investigated the proposed hybrid model. In order to evaluate the model performance, four commonly used statistical evolution indexes were utilized and five models, namely BPNN, SVM, LSTM, EMD-LSTM and VMD-LSTM, were used for comparison. The results indicated that the proposed model outperformed the five models in terms of all the four evolution indexes. Hence, the proposed method is feasible and promising for improving the forecasting accuracy of monthly runoff prediction.

Acknowledgements

This paper is supported by the National Natural Science Foundation of China (51709109).

Conflict of Interest

The authors declare that they have no known competing financial interests or personal relationships that could have appeared to influence the work reported in this paper

References

Altan, A., Karasu, S., Zio, E., 2021. A new hybrid model for wind speed forecasting combining long short-term memory neural network, decomposition methods and grey wolf optimizer. Appl Soft Comput, 100. DOI:10.1016/j.asoc.2020.106996

ASCE-Task-Committee, 2000. Artificial neural networks in hydrology-II: Hydrological applications. J Hydrol Eng, 5(2): 124-137.

Colominas, M.A., Schlotthauer, G., Torres, M.E., 2014. Improved complete ensemble EMD: A suitable tool for biomedical signal processing. Biomed Signal Process Control, 14: 19-29. DOI:10.1016/j.bspc.2014.06.009

Dakhlalla, A.O., Parajuli, P.B., 2016. Evaluation of the best management practices at the watershed scale to attenuate peak streamflow under climate change scenarios. Water Resour Manag, 30(3): 963-982. DOI:10.1007/s11269-015-1202-9

Dragomiretskiy, K., Zosso, D., 2014. Variational mode decomposition. IEEE Trans on Signal Process, 62(3): 531-544. DOI:10.1109/tsp.2013.2288675

ElSaid, A., El Jamiy, F., Higgins, J., Wild, B., Desell, T., 2018. Optimizing long short-term memory recurrent neural networks using ant colony optimization to predict turbine engine vibration. Appl Soft Comput, 73: 969-991. DOI:10.1016/j.asoc.2018.09.013

Fang, W., Huang, S., Ren, K., Huang, Q., Huang, G., Cheng, G., Li, K., 2019. Examining the applicability of different sampling techniques in the development of decomposition-based streamflow forecasting models. J Hydrol, 568: 534-550. DOI:10.1016/j.jhydrol.2018.11.020

Feng, Z.K., Niu, W.J., 2021. Hybrid artificial neural network and cooperation search algorithm for nonlinear river flow time series forecasting in humid and semi-humid regions. Knowl Based Syst, 211: 106580. DOI:10.1016/j.knosys.2020.106580

Feng, Z.K., Niu, W.J., Cheng, C.T., 2018. Optimization of hydropower reservoirs operation balancing generation benefit and ecological requirement with parallel multi-objective genetic algorithm.

426 ENERGY, 153: 706-718. DOI:10.1016/j.energy.2018.04.075
427 Feng, Z.K., Niu, W.J., Jiang, Z.Q., Qin, H., Song, Z.G., 2020a. Monthly operation optimization of
428 cascade hydropower reservoirs with dynamic programming and latin hypercube sampling for
429 dimensionality reduction. Water Resour Manag, 34(6): 2029-2041. DOI:10.1007/s11269-020-02545-
430 0
431 Feng, Z.K., Niu, W.J., Tang, Z.Y., Jiang, Z.Q., Xu, Y., Liu, Y., Zhang, H.R., 2020b. Monthly runoff time
432 series prediction by variational mode decomposition and support vector machine based on quantum-
433 behaved particle swarm optimization. J Hydrol, 583. DOI:10.1016/j.jhydrol.2020.124627
434 Feng, Z.K., Niu, W.J., Tang, Z.Y., Xu, Y., Zhang, H.R., 2021. Evolutionary artificial intelligence model
435 via cooperation search algorithm and extreme learning machine for multiple scales nonstationary
436 hydrological time series prediction. J Hydrol, 595. DOI:10.1016/j.jhydrol.2021.126062
437 Hochreiter, S., Schmidhuber, J., 1997. Long Short-Term Memory. Neural Comput, 9(8): 1735-1780.
438 DOI:10.1162/neco.1997.9.8.1735
439 Ji, C.-m., Zhou, T., Huang, H.-t., 2014. Operating rules derivation of Jinsha Reservoirs system with
440 parameter calibrated support vector regression. Water Resour Manag, 28(9): 2435-2451.
441 DOI:10.1007/s11269-014-0610-6
442 Kratzert, F., Klotz, D., Brenner, C., Schulz, K., Herrnegger, M., 2018. Rainfall-runoff modelling using
443 long short-term memory (LSTM) networks. Hydrol Earth Syst Sci, 22(11): 6005-6022.
444 DOI:10.5194/hess-22-6005-2018
445 Li, F.G., Ma, G.W., Chen, S.J., Huang, W.B., 2021. An ensemble modeling approach to forecast daily
446 reservoir inflow using bidirectional long- and short-term memory (Bi-LSTM), variational mode
447 decomposition (VMD), and energy entropy method. Water Resour Manag, 35(9): 2941-2963.
448 DOI:10.1007/s11269-021-02879-3
449 Li, Y., Wu, H., Liu, H., 2018. Multi-step wind speed forecasting using EWT decomposition, LSTM
450 principal computing, RELM subordinate computing and IEWT reconstruction. Energy Convers
451 Manag, 167: 203-219. DOI:10.1016/j.enconman.2018.04.082
452 Liao, S.L., Li, G., Sun, Q.Y., Li, Z.F., 2016. Real-time correction of antecedent precipitation for the
453 Xinanjiang model using the genetic algorithm. J Hydroinform, 18(5): 803-815.
454 DOI:10.2166/hydro.2016.168
455 Liao, S.L., Liu, Z.W., Liu, B.X., Cheng, C.T., Jin, X.F., Zhao, Z.P., 2020. Multistep-ahead daily inflow

456 forecasting using the ERA-Interim reanalysis data set based on gradient-boosting regression trees.
457 Hydrol Earth Syst Sci, 24(5): 2343-2363. DOI:10.5194/hess-24-2343-2020
458 Liu, H., Mi, X.W., Li, Y.F., 2018. Smart multi-step deep learning model for wind speed forecasting based
459 on variational mode decomposition, singular spectrum analysis, LSTM network and ELM. Energy
460 Convers Manag, 159: 54-64. DOI:10.1016/j.enconman.2018.01.010
461 Lv, N., Liang, X.X., Chen, C., Zhou, Y., Li, J., Wei, H., Wang, H., 2020. A long Short-Term memory
462 cyclic model with mutual information for hydrology forecasting: A Case study in the xixian basin.
463 Adv Water Resour, 141: 10. DOI:10.1016/j.advwatres.2020.103622
464 Madsen, H., 2003. Parameter estimation in distributed hydrological catchment modelling using
465 automatic calibration with multiple objectives. Adv Water Resour, 26(2): 205-216.
466 DOI:10.1016/s0309-1708(02)00092-1
467 Mirjalili, S., Mirjalili, S.M., Lewis, A., 2014. Grey wolf optimizer. Adv Eng Softw, 69: 46-61.
468 DOI:10.1016/j.advengsoft.2013.12.007
469 Nakisa, B., Rastgoo, M.N., Rakotonirainy, A., Maire, F., Chandran, V., 2018. Long short term memory
470 hyperparameter optimization for a neural network based emotion recognition framework. IEEE
471 Access, 6: 49325-49338. DOI:10.1109/access.2018.2868361
472 Ni, L., Wang, D., Singh, V.P., Wu, J., Wang, Y., Tao, Y., Zhang, J., 2020. Streamflow and rainfall
473 forecasting by two long short-term memory-based models. J Hydrol, 583: 124296.
474 DOI:10.1016/j.jhydrol.2019.124296
475 Niu, W.J., Feng, Z.K., Liu, S., Chen, Y.B., Xu, Y.S., Zhang, J., 2021. Multiple hydropower reservoirs
476 operation by hyperbolic grey wolf optimizer based on elitism selection and adaptive mutation. Water
477 Resour Manag, 35(2): 573-591. DOI:10.1007/s11269-020-02737-8
478 Niu, W.j., Feng, Z.k., Zeng, M., Feng, B.f., Min, Y.W., Cheng, C.T., Zhou, J.Z., 2019. Forecasting
479 reservoir monthly runoff via ensemble empirical mode decomposition and extreme learning machine
480 optimized by an improved gravitational search algorithm. Appl Soft Comput, 82: 105589.
481 DOI:10.1016/j.asoc.2019.105589
482 Nourani, V., Alami, M.T., Aminfar, M.H., 2009. A combined neural-wavelet model for prediction of
483 Ligvanchai watershed precipitation. Eng Appl of Arti Intell, 22(3): 466-472.
484 DOI:10.1016/j.engappai.2008.09.003
485 Nuaekaew, K., Artrit, P., Pholdee, N., Bureerat, S., 2017. Optimal reactive power dispatch problem using

a two-archive multi-objective grey wolf optimizer. Expert Syst Appl, 87: 79-89. DOI:10.1016/j.eswa.2017.06.009

Roushangar, K., Ghasempour, R., Nourani, V., 2021. The potential of integrated hybrid pre-post-processing techniques for short- to long-term drought forecasting. J Hydroinform, 23(1): 117-135. DOI:10.2166/hydro.2020.088

Şen, Z., 2021. Reservoirs for water supply under climate change impact—A Review. Water Resour Manag, 35(11): 3827-3843. DOI:10.1007/s11269-021-02925-0

Seo, Y., Kim, S., Kisi, O., Singh, V.P., 2015. Daily water level forecasting using wavelet decomposition and artificial intelligence techniques. J Hydrol, 520: 224-243. DOI:10.1016/j.jhydrol.2014.11.050

Shoaib, M., Shamseldin, A.Y., Khan, S., Khan, M.M., Khan, Z.M., Sultan, T., Melville, B.W., 2018. A comparative study of various hybrid wavelet feedforward neural network models for runoff forecasting. Water Resour Manag, 32(1): 83-103. DOI:10.1007/s11269-017-1796-1

Sibtain, M., Li, X.S., Bashir, H., Azam, M.I., 2021. A hybrid model for runoff prediction using variational mode decomposition and artificial neural network. Water Resour, 48(5): 701-712. DOI:10.1134/s0097807821050171

Tikhamarine, Y., Souag-Gamane, D., Ahmed, A.N., Kisi, O., El-Shafie, A., 2020. Improving artificial intelligence models accuracy for monthly streamflow forecasting using grey Wolf optimization (GWO) algorithm. J Hydrol, 582. DOI:10.1016/j.jhydrol.2019.124435

Wan, F., Wang, F.Q., Yuan, W.L., 2017. The reservoir runoff forecast with artificial neural network based on ant colony optimization. Appl Ecol and Environ Res, 15(4): 497-510. DOI:10.15666/aeer/1504_497510

Wang, W.C., Chau, K.W., Xu, D.M., Chen, X.Y., 2015. Improving forecasting accuracy of annual runoff time series using ARIMA based on EEMD decomposition. Water Resour Manag, 29(8): 2655-2675. DOI:10.1007/s11269-015-0962-6

Wang, X.J., Wang, Y.P., Yuan, P.X., Wang, L., Cheng, D.L., 2021. An adaptive daily runoff forecast model using VMD-LSTM-PSO hybrid approach. Hydrol Sci J, 66(9): 1488-1502. DOI:10.1080/02626667.2021.1937631

Wang, Y.X., Liu, F.Y., Jiang, Z.S., He, S.L., Mo, Q.Y., 2017. Complex variational mode decomposition for signal processing applications. Mech Syst Signal Process, 86: 75-85. DOI:10.1016/j.ymssp.2016.09.032

Wu, C.L., Chau, K.W., 2011. Rainfall-runoff modeling using artificial neural network coupled with singular spectrum analysis. J Hydr, 399(3-4): 394-409. DOI:10.1016/j.jhydrol.2011.01.017

Xu, B., Boyce, S.E., Zhang, Y., Liu, Q., Guo, L., Zhong, P.-A., 2017. Stochastic programming with a joint chance constraint model for reservoir refill operation considering flood risk. J Water Resour Plan Manag, 143(1): 04016067. DOI:doi:10.1061/(ASCE)WR.1943-5452.0000715

Yu, J., Wang, S., Xi, L., 2008. Evolving artificial neural networks using an improved PSO and DPSO. Neurocomputing, 71(4): 1054-1060. DOI:10.1016/j.neucom.2007.10.013

Yuan, X.H., Chen, C., Lei, X.H., Yuan, Y.B., Adnan, R.M., 2018. Monthly runoff forecasting based on LSTM-ALO model. Stoch Environ Res Risk Assess, 32(8): 2199-2212. DOI:10.1007/s00477-018-1560-y

Zhang, M., Jiang, Z.N., Feng, K., 2017. Research on variational mode decomposition in rolling bearings fault diagnosis of the multistage centrifugal pump. Mech Syst Signal Process, 93: 460-493. DOI:10.1016/j.ymssp.2017.02.013

Zuo, G.G., Luo, J.G., Wang, N., Lian, Y.N., He, X.X., 2020. Decomposition ensemble model based on variational mode decomposition and long short-term memory for streamflow forecasting. J Hydrol, 585. DOI:10.1016/j.jhydrol.2020.124776

Figures

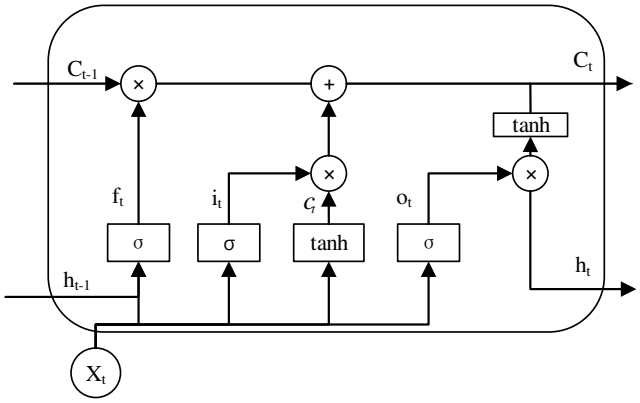

Fig. 1 Schematic diagram of long short-term memory neural networks

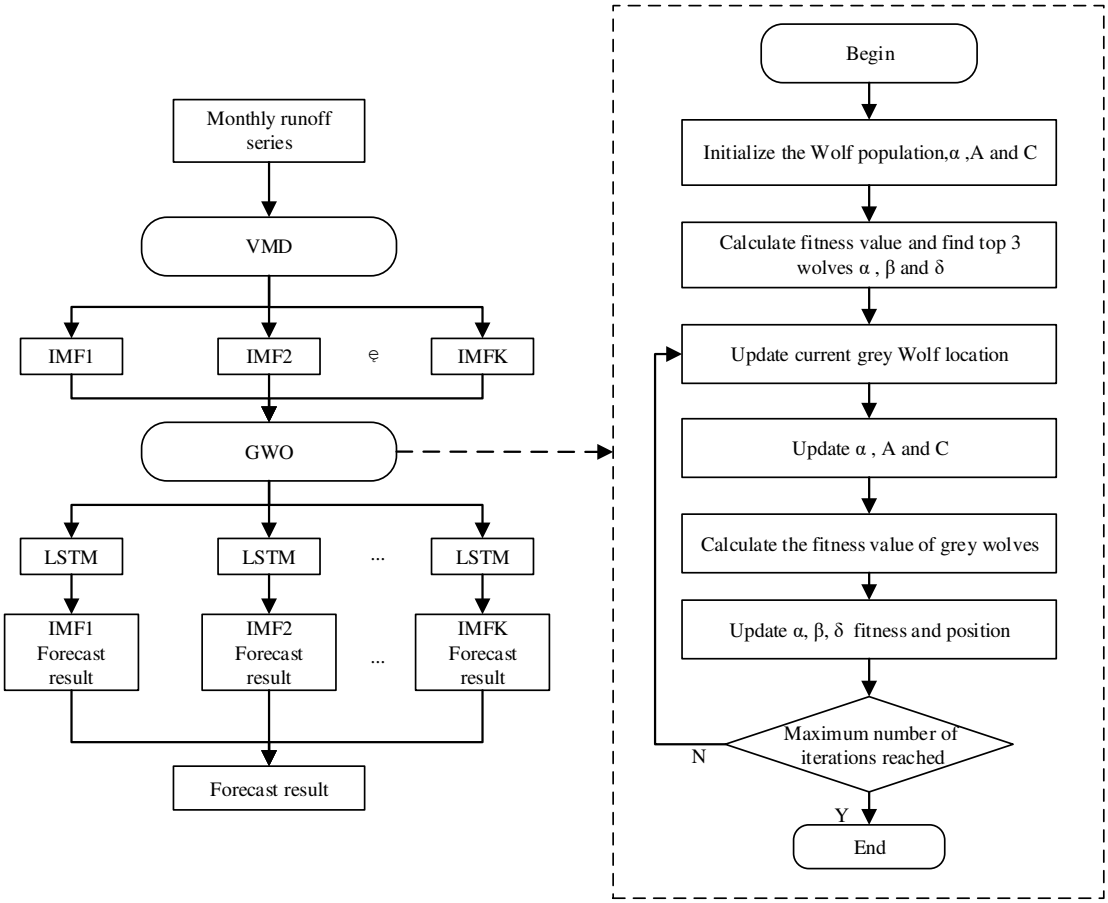

563

564 Fig. 2 The flowchart of VMD-GWO-LSTM for monthly runoff forecasting

565

566

567 Fig. 3 Location of the Xinfengjiang and Guangzhao Reservoirs in China

568

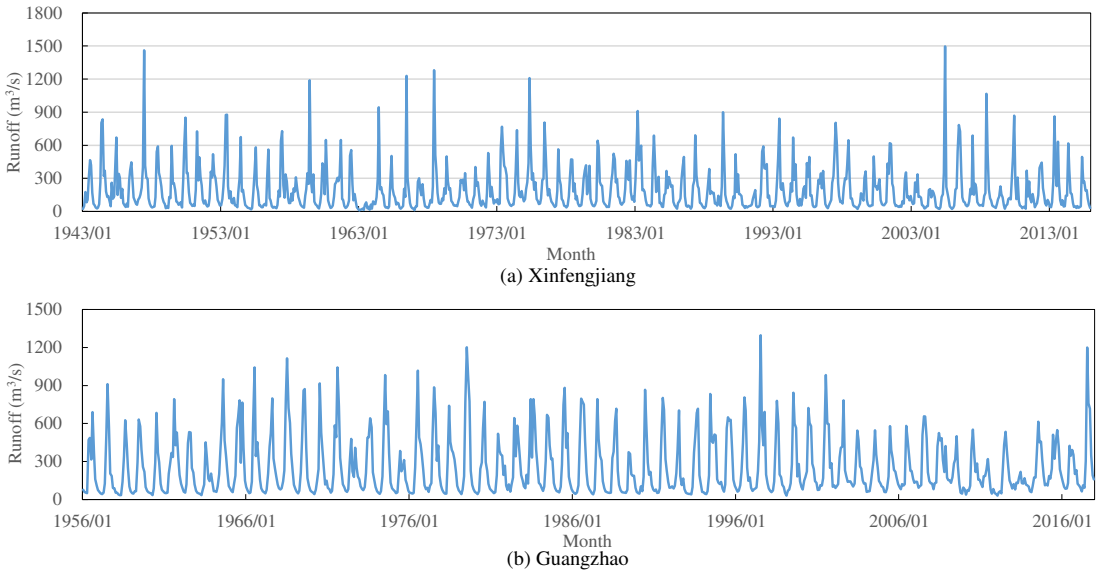

(a) Xinfengjiang

(b) Guangzhao

569

570 Fig. 4 Monthly runoff hydrograph of the Xinfengjiang and Guangzhao Reservoirs

571

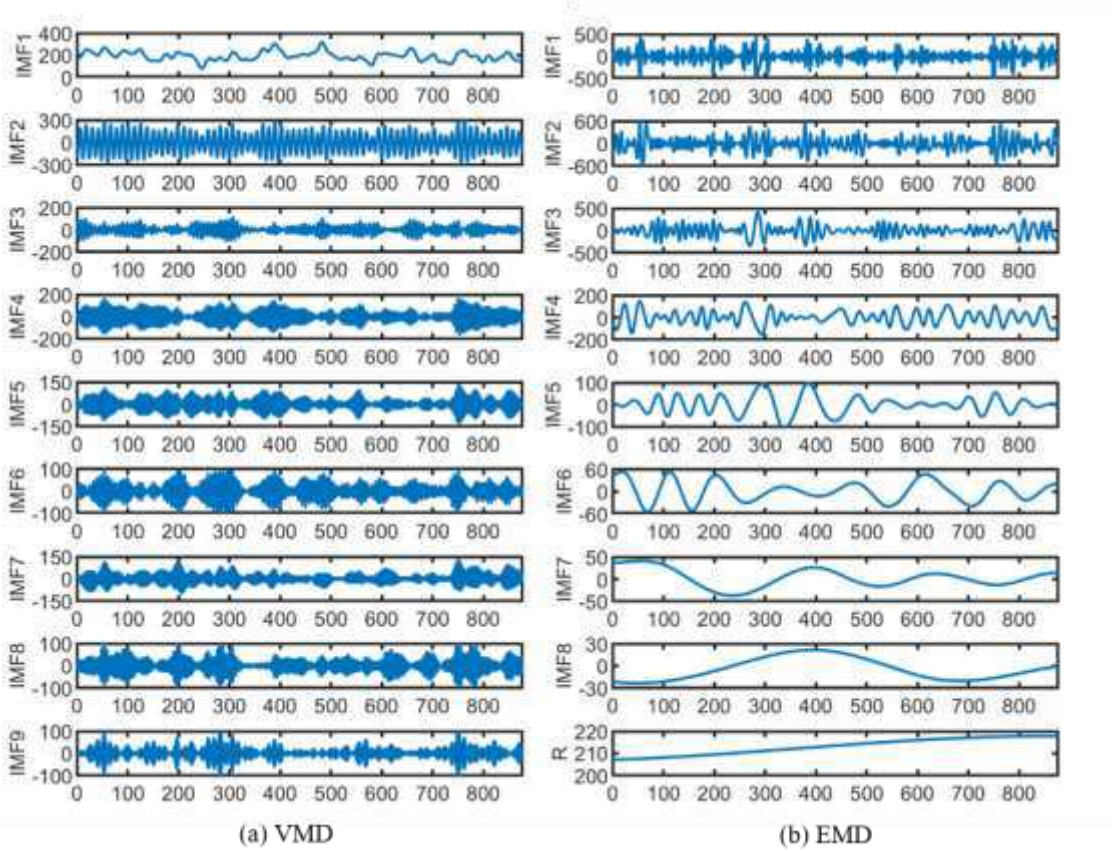

572

573 Fig. 5 Decomposed results of monthly runoff data in Xinfengjiang Reservoirs

574

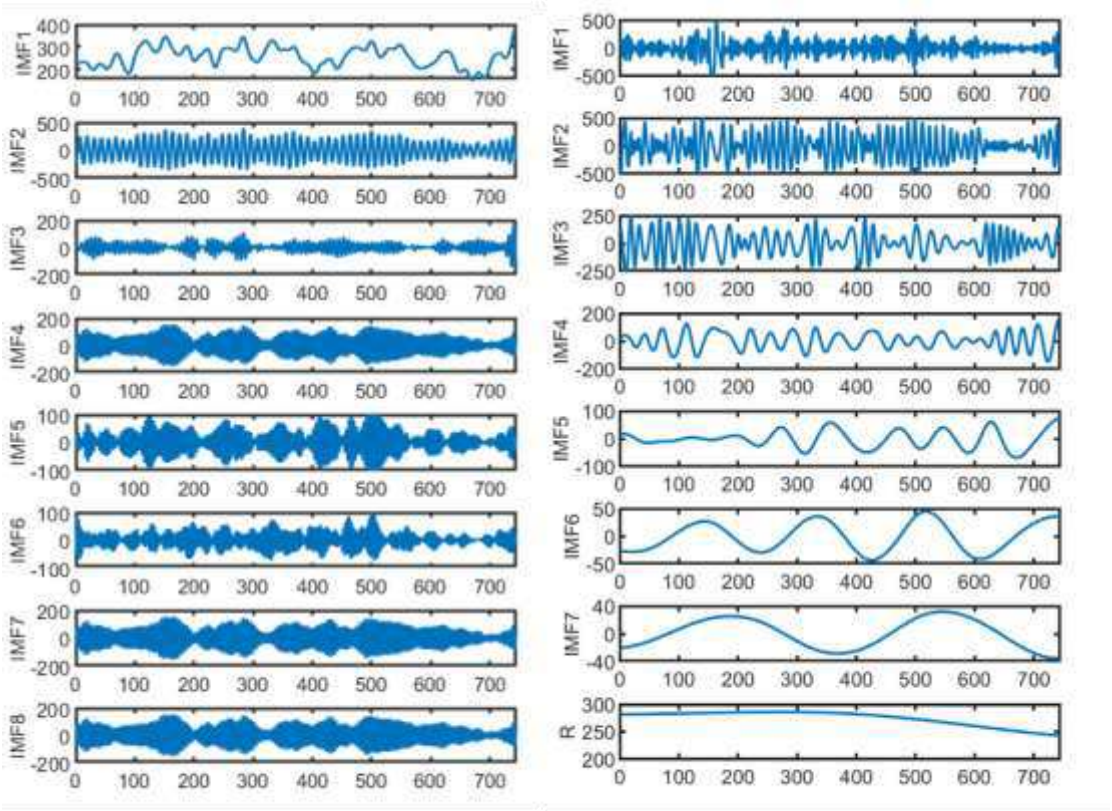

575

576 Fig. 6 Decomposed results of monthly runoff data in Guangzhao Reservoirs

577

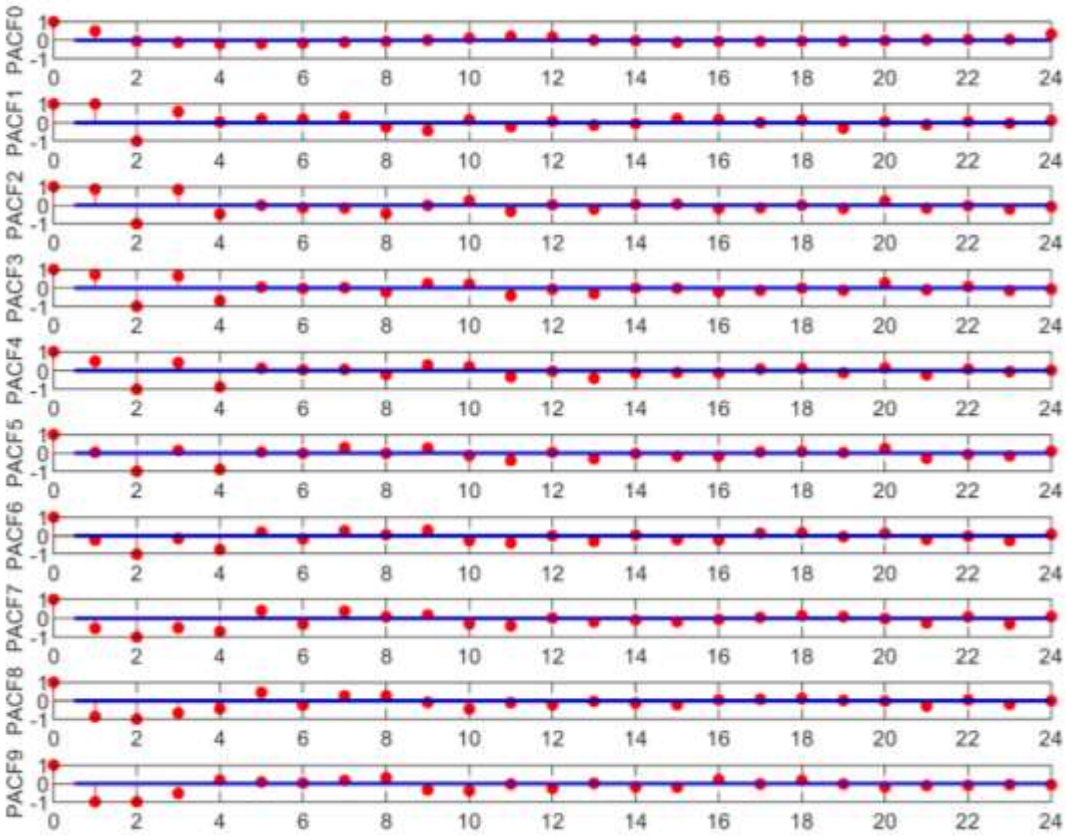

578

579 Fig. 7 PACF values of each series from the Xinfengjiang Reservoir

580

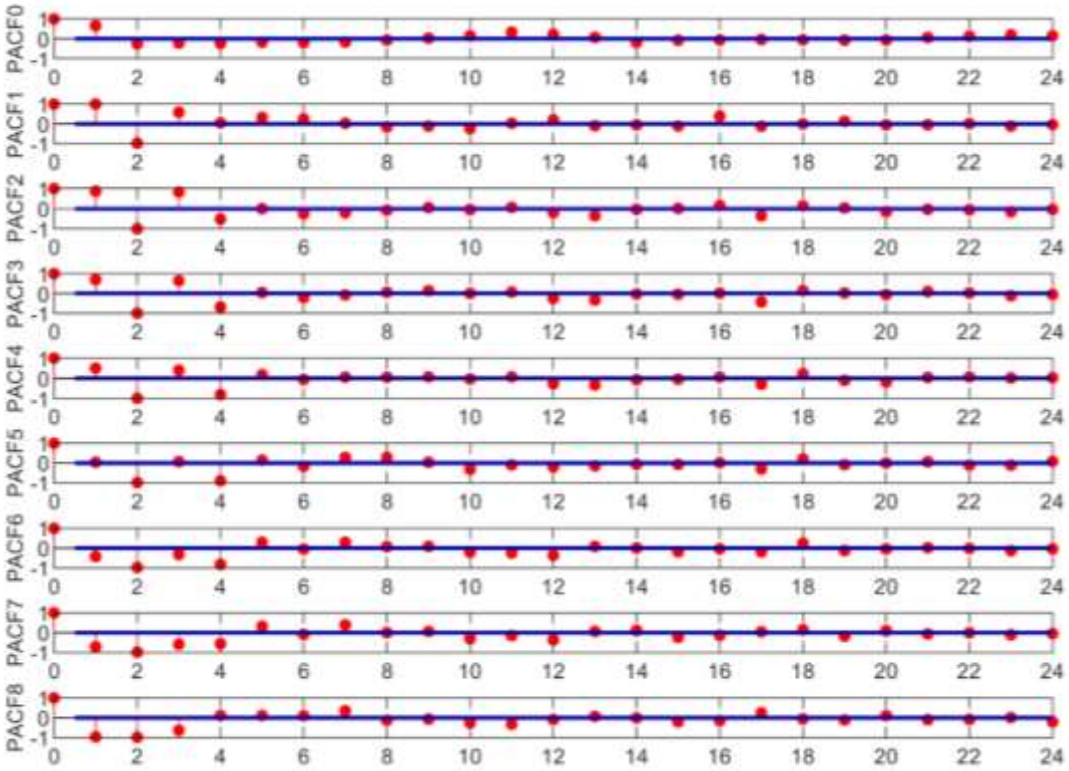

581

582 Fig. 8 PACF values of each series from the Guangzhao Reservoir

583

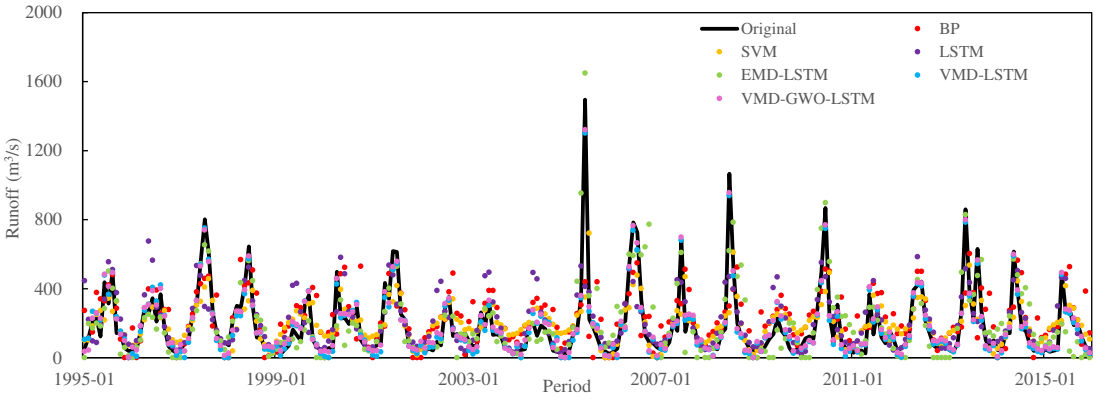

584

585 Fig.9 Comparison of the forecast results for the Xinfengjiang Reservoir during the validation period

586

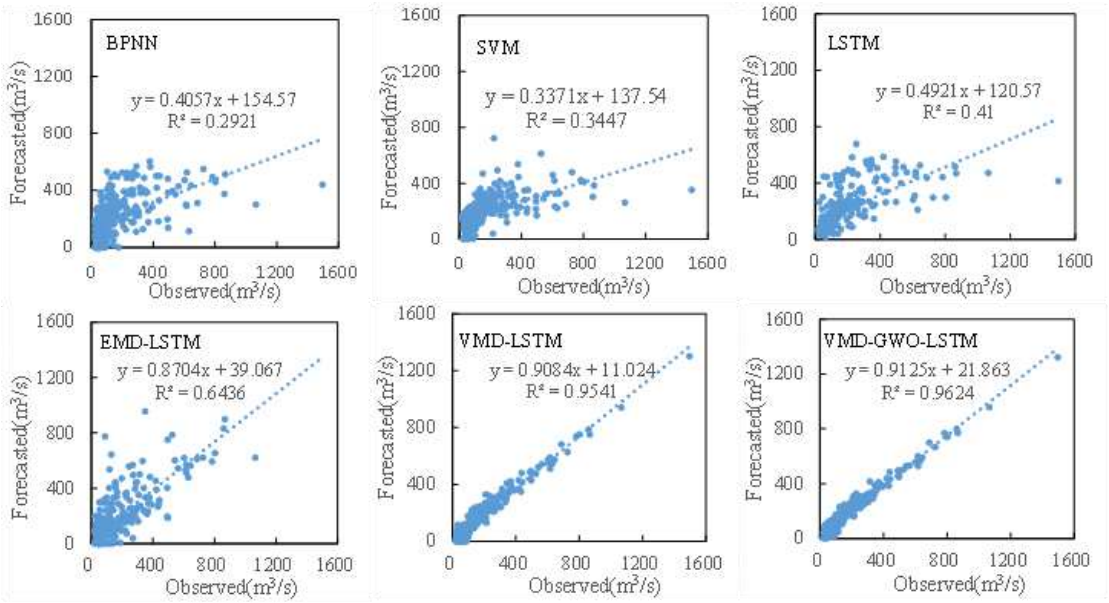

587

588 Fig. 10 Comparison of scatter diagrams of forecast results for the Xinfengjiang Reservoir during the

589 validation period

590

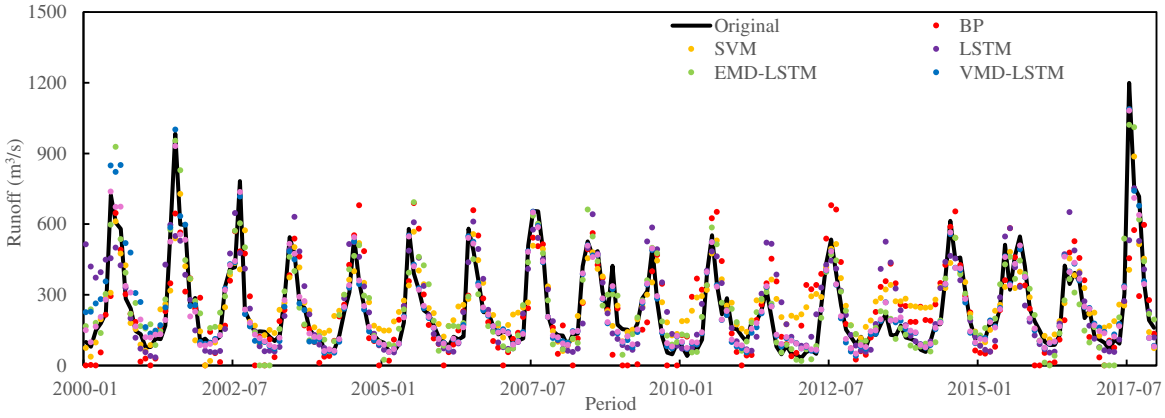

591

592 Fig.11 Comparison of the forecast results for the Guangzhao Reservoir during the validation period

593

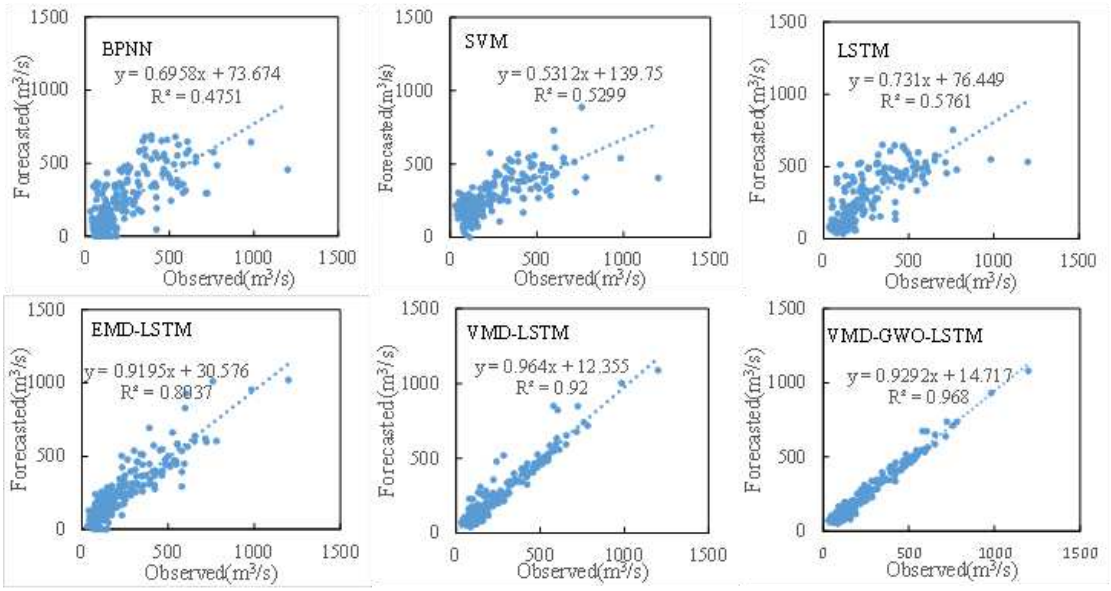

Fig. 12 Comparison of scatter diagrams of forecast results during the validation period for the Guangzhao Reservoir

Tables

608 Table 1 The selected input values of each series for the Xinfengjiang Reservoir monthly runoff data

No.	Series	Input variables	Numbers of input
1	Original	x_{t-1}, x_{t-2}, x_{t-3}, x_{t-4}, x_{t-5}, x_{t-6}, x_{t-7}, x_{t-8}	8
2	IMF_1	x_{t-1}, x_{t-2}, x_{t-3}	3
3	IMF_2	x_{t-1}, x_{t-2}, x_{t-3}, x_{t-4}	4
4	IMF_3	x_{t-1}, x_{t-2}, x_{t-3}, x_{t-4}	4
5	IMF_4	x_{t-1}, x_{t-2}, x_{t-3}, x_{t-4}	4
6	IMF_5	x_{t-1}, x_{t-2}, x_{t-3}, x_{t-4}	4
7	IMF_6	x_{t-1}, x_{t-2}, x_{t-3}, x_{t-4}, x_{t-5}, x_{t-6}, x_{t-7}	7
8	IMF_7	x_{t-1}, x_{t-2}, x_{t-3}, x_{t-4}, x_{t-5}, x_{t-6}, x_{t-7}	7
9	IMF_8	x_{t-1}, x_{t-2}, x_{t-3}, x_{t-4}, x_{t-5}, x_{t-6}, x_{t-7}, x_{t-8}	8
10	IMF_9	x_{t-1}, x_{t-2}, x_{t-3}, x_{t-4}	4

609

610

611 Table 2 The selected input values of each series for the Guangzhao Reservoir monthly runoff data

No.	Series	Input variables	Numbers of input
1	Original	x_{t-1}, x_{t-2}, x_{t-3}, x_{t-4}, x_{t-5}, x_{t-6}, x_{t-7}	7
2	IMF_1	x_{t-1}, x_{t-2}, x_{t-3}	3
3	IMF_2	x_{t-1}, x_{t-2}, x_{t-3}, x_{t-4}	4
4	IMF_3	x_{t-1}, x_{t-2}, x_{t-3}, x_{t-4}	4
5	IMF_4	x_{t-1}, x_{t-2}, x_{t-3}, x_{t-4}, x_{t-5}	5
6	IMF_5	x_{t-1}, x_{t-2}, x_{t-3}, x_{t-4}, x_{t-5}, x_{t-6}, x_{t-7}, x_{t-8}	8
7	IMF_6	x_{t-1}, x_{t-2}, x_{t-3}, x_{t-4}, x_{t-5}	5
8	IMF_7	x_{t-1}, x_{t-2}, x_{t-3}, x_{t-4}, x_{t-5}	5
9	IMF_8	x_{t-1}, x_{t-2}, x_{t-3}, x_{t-4}	4

612

613

614 Table 3 Comparison of evaluation indexes of different models for the Xinfengjiang Reservoir

Models	Calibration				Validation			
	RMSE	MAPE	R	CE	RMSE	MAPE	R	CE
BPNN	176.912	116.940	0.558	0.245	175.616	124.456	0.540	0.193
SVM	162.401	92.020	0.604	0.364	159.082	95.410	0.587	0.338
LSTM	143.215	73.108	0.713	0.505	154.706	76.900	0.640	0.373
EMD-LSTM	76.179	52.945	0.931	0.861	130.014	81.677	0.802	0.557
VMD-LSTM	39.524	30.710	0.984	0.962	43.224	32.676	0.977	0.951
VMD-GWO-LSTM	36.950	29.348	0.985	0.967	38.720	30.395	0.981	0.961

615

616

617

618 Table 4 Peak flow estimates of different models for the Xinfengjiang Reservoir during the validation

619 period

Peak NO.	Observed peaks (m^3/s)	BPNN (m^3/s)	SVM (m^3/s)	LSTM (m^3/s)	EMD-LSTM (m^3/s)	VMD-LSTM (m^3/s)	VMD-GWO-LSTM(m^3/s)	Relative error(%)					
								BPNN	SVM	LSTM	EMD-LSTM	VMD-LSTM	VMD-GWO-LSTM
1	494.0	481.1	269.0	510.0	402.1	493.5	492.3	-2.6	-45.6	3.2	-18.6	-0.1	-0.4
2	368.0	256.2	232.6	247.6	235.6	421.4	401.5	-30.4	-36.8	-32.7	-36.0	14.5	9.1
3	803.0	458.8	408.5	296.9	653.2	751.2	739.4	-42.9	-49.1	-63.0	-18.7	-6.5	-7.9
4	645.0	433.9	329.2	524.6	561.6	572.8	589.8	-32.7	-49.0	-18.7	-12.9	-11.2	-8.6
5	362.0	385.8	311.7	145.4	212.9	388.7	385.6	6.6	-13.9	-59.8	-41.2	7.4	6.5
6	498.0	137.4	168.3	265.3	184.4	427.3	459.2	-72.4	-66.2	-46.7	-63.0	-14.2	-7.8
7	618.0	526.7	324.4	479.4	508.7	508.8	526.4	-14.8	-47.5	-22.4	-17.7	-17.7	-14.8
8	353.0	381.8	319.9	233.4	335.3	332.6	344.2	8.2	-9.4	-33.9	-5.0	-5.8	-2.5
9	336.0	389.9	239.5	495.3	243.1	303.6	332.8	16.0	-28.7	47.4	-27.7	-9.7	-0.9
10	203.0	319.8	280.4	493.7	197.4	255.8	275.6	57.6	38.1	143.2	-2.8	26.0	35.8
11	1496.0	439.3	351.0	412.9	1649.7	1301.1	1321.0	-70.6	-76.5	-72.4	10.3	-13.0	-11.7
12	783.8	493.5	422.4	441.7	592.1	738.2	766.3	-37.0	-46.1	-43.6	-24.5	-5.8	-2.2
13	687.5	311.7	251.4	436.1	610.4	680.8	698.2	-54.7	-63.4	-36.6	-11.2	-1.0	1.6
14	1066.0	299.6	260.5	470.4	619.8	940.2	956.8	-71.9	-75.6	-55.9	-41.9	-11.8	-10.2
15	228.2	278.9	252.5	468.5	159.9	320.0	325.4	22.2	10.6	105.3	-29.9	40.2	42.6
16	867.5	512.7	382.7	469.6	897.9	748.6	769.1	-40.9	-55.9	-45.9	3.5	-13.7	-11.3
17	369.6	176.1	186.8	408.9	291.8	394.0	409.8	-52.3	-49.4	10.6	-21.0	6.6	10.9
18	442.3	500.5	352.2	424.0	313.4	414.8	433.3	13.2	-20.4	-4.1	-29.1	-6.2	-2.0
19	860.9	374.5	302.5	515.3	829.3	785.5	799.0	-56.5	-64.9	-40.1	-3.7	-8.8	-7.2
20	616.2	292.6	233.3	450.7	570.9	589.3	599.8	-52.5	-62.1	-26.9	-7.4	-4.4	-2.7
21	493.6	196.4	214.6	465.0	195.6	482.8	493.6	-60.2	-56.5	-5.8	-60.4	-2.2	0.0
Average (absolute)								38.9	46.0	43.7	23.2	10.8	9.4

620

621

622 Table 5 Comparison of evaluation indexes of different models for the Guangzhao Reservoir

Models	Calibration				Validation			
	RMSE	MAPE	R	CE	RMSE	MAPE	R	CE
BPNN	162.371	73.088	0.762	0.570	148.575	67.225	0.689	0.373
SVM	157.653	69.643	0.771	0.595	131.621	66.394	0.728	0.508
LSTM	134.204	32.806	0.845	0.706	128.575	50.008	0.759	0.530
EMD-LSTM	105.202	55.066	0.941	0.884	87.303	36.484	0.897	0.783
VMD-LSTM	39.146	19.660	0.989	0.975	53.880	22.798	0.959	0.917
VMD-GWO-LSTM	37.987	17.572	0.990	0.976	34.415	17.921	0.984	0.966

623
624

625 Table 6 Peak flow estimates of different models for the Guangzhao Reservoir during the validation period

Peak NO.	Observed peaks (m^3/s)	BPNN (m^3/s)	SVM (m^3/s)	LSTM (m^3/s)	EMD-LSTM (m^3/s)	VMD-LSTM (m^3/s)	VMD-GWO-LSTM (m^3/s)	Relative error(%)					
								BP	SVM	LSTM	EMD-LSTM	VMD-LSTM	VMD-GWO-LSTM
1	723.5	293.8	308.1	454.3	597.1	848.7	738.2	-59.4	-57.4	-37.2	-17.5	17.3	2.0
2	983.3	644.1	539.3	548.6	953.6	1001.5	931.1	-34.5	-45.2	-44.2	-3.0	1.9	-5.3
3	782.6	484.0	407.5	477.1	603.5	717.1	736.4	-38.1	-47.9	-39.0	-22.9	-8.4	-5.9
4	544.8	382.6	373.4	490.3	460.7	483.8	515.7	-29.8	-31.5	-10.0	-15.4	-11.2	-5.3
5	546.4	552.6	399.6	523.2	465.2	525.7	544.5	1.1	-26.9	-4.3	-14.9	-3.8	-0.4
6	580.2	357.1	339.5	487.2	393.0	551.0	546.7	-38.5	-41.5	-16.0	-32.3	-5.0	-5.8
7	580.5	295.9	282.2	437.2	291.8	547.9	541.0	-49.0	-51.4	-24.7	-49.7	-5.6	-6.8
8	656.2	542.0	508.2	576.5	635.7	653.0	649.6	-17.4	-22.6	-12.2	-3.1	-0.5	-1.0
9	526.0	492.7	454.3	497.9	661.7	510.0	508.3	-6.3	-13.6	-5.4	25.8	-3.1	-3.4
10	500.2	399.0	352.0	585.4	498.6	489.4	495.6	-20.2	-29.6	17.0	-0.3	-2.1	-0.9
11	552.7	624.3	474.3	483.4	584.9	523.9	523.3	13.0	-14.2	-12.5	5.8	-5.2	-5.3
12	320.4	347.6	327.5	521.3	311.4	332.4	336.4	8.5	2.2	62.7	-2.8	3.7	5.0
13	535.0	679.8	495.1	445.0	471.0	484.7	483.7	27.1	-7.5	-16.8	-12.0	-9.4	-9.6
14	219.9	357.1	321.9	524.8	224.6	267.4	266.9	62.4	46.4	138.6	2.1	21.6	21.4
15	614.1	588.4	434.5	464.8	563.2	556.8	564.1	-4.2	-29.2	-24.3	-8.3	-9.3	-8.1
16	548.0	338.2	397.4	333.6	444.7	493.3	508.5	-38.3	-27.5	-39.1	-18.8	-10.0	-7.2
17	423.9	191.3	263.8	471.5	275.8	465.2	461.9	-54.9	-37.8	11.2	-34.9	9.7	9.0
18	1199.6	454.5	405.7	531.1	1021.1	1087.9	1081.4	-62.1	-66.2	-55.7	-14.9	-9.3	-9.9
Average (absolute)								31.4	33.2	31.7	15.8	7.6	6.2

626
627
628
629
630
631